# DEVELOPMENT OF THE DLR TAU CODE FOR MODELLING OF CONTROL SURFACES

L. Alcaraz Capsada, R. Heinrich

German Aerospace Center (DLR), Institute of Aerodynamics and Flow Technology

Lilienthalplatz 7, 38108 Braunschweig

Germany

## Abstract

The simulation of movable control surfaces is of interest for many applications in aerospace engineering, but it is challenging to perform high-fidelity computations considering them. Generating a new mesh for each deflection angle is computationally expensive and not suitable for dynamically moving control surfaces, so alternative approaches that allow using only one mesh have been developed in the recent years. This work gives an overview of the available methods for modelling of control surfaces, with special focus on the ones that consider the spanwise gaps between the wing and the control surface. This includes the usage of the Chimera technique combined with mesh deformation as well as a sliding interfaces boundary condition.

## Keywords

Computational Fluid Dynamics, control surfaces, mesh generation

## Nomenclature

| | | | |
|---|---|---|---|
| $C_L$: | Lift force coefficient | $Re_\infty$: | Farfield Reynolds number |
| $C_p$: | Pressure coefficient | $\alpha$: | Angle of attack |
| $C_{ref}$: | Reference chord length | $\delta$: | Deflection angle of the control surface |
| $Ma_\infty$: | Farfield Mach number | | |

## 1. INTRODUCTION

High-fidelity Computational Fluid Dynamics (CFD) methods based on solving the Unsteady Reynolds-averaged Navier-Stokes (URANS) equations are regarded as an important tool for aerodynamics prediction and analysis during the aircraft design process. Nowadays, it is desired to have a realistic digital model of an aircraft which can be used for virtual design, virtual flight testing and, ultimately, for virtual certification. Among others, this requires developing the CFD features to consider the complete flight envelope, improving the capabilities of High Performance Computing (HPC) or considering complex geometries like high-lift systems or movable control surfaces. Thanks to the maturity of the CFD algorithms and the improvements in mesh generation techniques, the simulation of control surfaces with fixed deflections has become a standard procedure. Nevertheless, it is still challenging to predict the flow around a movable control surface. The main difficulty consists in developing methods to perform computations which are accurate, robust and efficient.

Capturing the aerodynamic impact of deflecting the control surfaces is of great importance during the design process of an aircraft, for instance to predict its manoeuvrability or design a Gust Load Alleviation (GLA) system. Other applications that require the handling of control surfaces are the generation of aerodynamic data bases or the performance of flight dynamic investigations, for example through virtual flights. Therefore, it is necessary to predict the influence of control surface deflections on the force and moment coefficients of the aircraft, and also to quantify the related loads. This provides information about the controllability of the aircraft, its hinge moments or the

effectiveness of the control surface.

In the recent years, efforts to model control surfaces with CFD have been carried out in several projects like ComFlite or Digital-X [1], and more recently, in VicToria or Mephisto. Within these projects, the capabilities of the DLR flow solver TAU [2] have been extended to perform efficient simulations, that is, to avoid generating a new computational mesh for each deflection angle of the control surface. One possibility is to use a mesh deformation method to move the nodes of the mesh in the area of the control surface, but this method cannot model the narrow spanwise gaps between the control surface and the wing of the aircraft, which are of interest from an aerodynamic point of view. These gaps can be modelled using the standard Chimera technique. To guarantee a valid Chimera mesh, an additional gap in flow direction has to be considered. However, in reality this gap is very small or even not present, and has no physical meaning. Against this backdrop, it is required to develop alternative strategies which only take into account the spanwise gaps.

This work describes the methods for modelling of control surfaces used at DLR. First, the so-called basic methods, i.e., remeshing, the usage of the Chimera technique or mesh deformation, are shown. Then, two alternative strategies are presented. The first one consists in a combination of mesh deformation and the Chimera technique, while the second one is a combination of mesh deformation and sliding interfaces, a new boundary condition that has been implemented in TAU. In the last part of this work, a comparison between the two methods is done. In addition, the verification of the new boundary condition is presented and the influence of the spanwise gaps on the aerodynamics of a wing is investigated.

## 2. BASIC METHODS

### 2.1. Modification of the CAD geometry and remeshing

The simplest way to model the deflection of a flap is to modify the Computer-Aided-Design (CAD) geometry of the configuration and then create a new computational mesh. This provides very realistic geometries and good-quality meshes, thus an accurate flow solution is expected. However, this method is very inefficient and time consuming because it requires generating a new mesh for each deflection angle of the control surface. The connectivity of each mesh is different, so remeshing is not suitable for performing dynamic simulations with movable control surfaces.

The important drawbacks of working with many meshes make necessary to develop alternative methods where only one mesh is used, as presented below.

### 2.2. Mesh deformation

The usage of mesh deformation is the simplest alternative to the remeshing approach, especially in the case of moderate deflection angles which will not result in meshes with bad quality elements that can negatively influence the quality and stability of the CFD computation. In this work, mesh deformation based on Radial Basis Functions (RBF) is used; however other mesh deformation techniques could also be used.

RBF-based mesh deformation has many convenient features that have helped to increase the popularity of the method in the recent years. Among others, RBF mesh deformation provides high-quality meshes while reasonably preserving its orthogonality near the deformation boundaries, does not need any connectivity information and allows the interpolation of arbitrary scattered data (base points). Given a surface mesh component, the RBF mesh deformation approach performs a polynomial interpolation of a surface displacement field, which is then evaluated at all volume mesh points. The interpolants are based on a set of scattered data which consists of the coordinates of the base points and the value of the corresponding displacements. In the following, the computation of the displacement field is briefly described. A detailed explanation of the RBF deformation method is given in [3].

During the mesh deformation process, the surface mesh components are classified into those which are kept fixed (the wing) and those which are deflected (the control surfaces). For the fixed components, four non-planar points are defined, and the corresponding displacement vectors are explicitly set to zero. For the second group, a set of equidistant points are placed on the surface mesh components. The computation of the displacement vectors depends on whether these points belong to the so-called expansion or compression side of the control surface. In the case of downward deflections ($\delta > 0$), the expansion side corresponds to the upper part of the control surface, while the compression one corresponds to its lower side, see figure 1.

The displacement field of the expansion side is computed according to the so-called hinge blending method from [4]. This method helps to generate smooth surface meshes that are also mechanically-representative of the deployment of a real control surface. The method consists

in centering a virtual cylinder along the hinge line and then requiring the surface mesh to smoothly lie on it as the nodes are stretched due to the expanding surface. Not all the nodes of the deformed mesh will lie on the cylinder, so a smooth surface until the aileron´s trailing edge must be ensured. Since the part of the surface mesh that does not belong to the control surface is explicitly set fixed during the deformation procedure, special diligence is needed to achieve a smooth transition between the fixed and the deformed part of the mesh. The hinge blending method guarantees a good quality surface mesh on the expansion side of the wing, but degenerated elements close to the kink are usually found on the compression side. In order to avoid this, the deflection field on the compression side of the control surface is generated through linear interpolation.
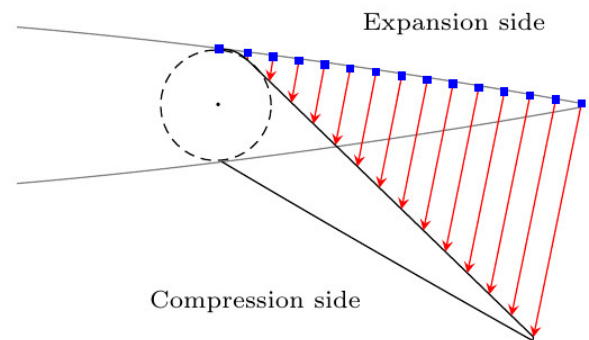


Figure 1: Computation of the displacement field at the base points on the expansion side of a generic control surface.

It is not recommended to model the spanwise gaps between the wing and the control surface when using mesh deformation, since the procedure is very likely to produce highly sheared elements in the gap areas even at low deflection angles. Then, the mesh will have bad quality elements or even cells with negative volumes, which will affect the flow computation. In order to avoid this, a blending function is applied to guarantee a lateral smooth transition between the wing and the control surface, as shown in figure 2.
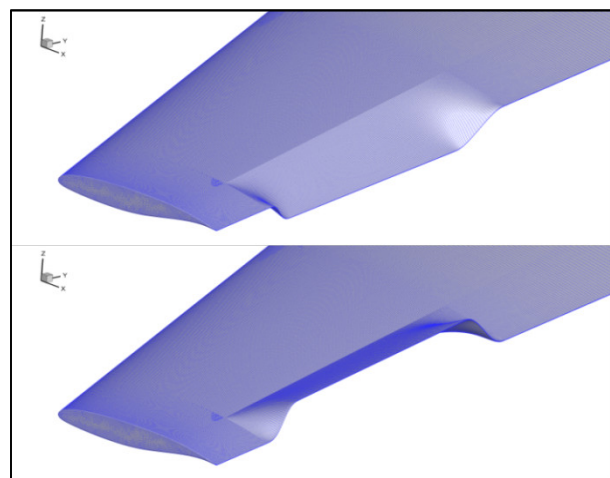


Figure 2: 30° downward and upward deflection of a control surface with mesh deformation.

## 2.3. Chimera technique

The usage of the Chimera technique [5], also known as overset mesh method, requires assembling several component meshes that overlap each other. The computation of a flow solution is done by communication (data interpolation) between the different meshes. With the Chimera technique, efficient simulations of relative motion between bodies can be done, so it is also suitable to simulate movable control surfaces. Besides, the flexibility of the mesh generation in the case of complex configurations is increased. An example of how the Chimera technique can be used for this purpose is shown in figure 3. The mesh is made of a mesh for the wing and a mesh for the flap, which can be rigidly-rotated to perform simulations with different deflection angles. Since the elements are not deformed, the quality of the mesh is kept and simulations with large deflection angles can be performed.

Using the Chimera technique and a rigid motion to rotate a flap requires considering narrow gaps between the meshes in both flow and span directions, that is, the control surface is "discrete". Although the presence of a gap in flow direction helps to delay stall, the large performance losses at low angles of attack, which usually occur in cruise flight, discourage using discrete flaps [6]. In reality, the gap is usually sealed. Thus, this gap can be considered non-physical and is only necessary to enable the usage of the Chimera technique.

The main constraint of the Chimera technique is the requirement of a sufficient overlap between the different mesh components. The overlap region is of great importance because in this region the data transfer between the mesh components occurs, and its size is related to the degree of interpolation. Therefore, an insufficient overlap decreases the degree of interpolation down to zero, and the flow solution is locally degraded. Due to the overlap constraint, the generation of a Chimera mesh is usually a difficult process and requires experienced users. In addition, it can result in very fine meshes within the gaps, and in the areas close to them.

The so-called hole definition geometry is also required during the computation and has to be provided by the user. It is responsible for marking (blanking) the nodes of the wing/flap mesh that are located inside the flap/wing,

which have to be excluded from the solution process. Due to the narrow gaps, it is not straight forward to create a hole definition geometry which still guarantees a sufficient overlap for interpolation between the meshes. Sometimes orphan points are found. In this case, using the automatic hole-cutting procedure that has recently been implemented in TAU [7] can decrease the user effort required.
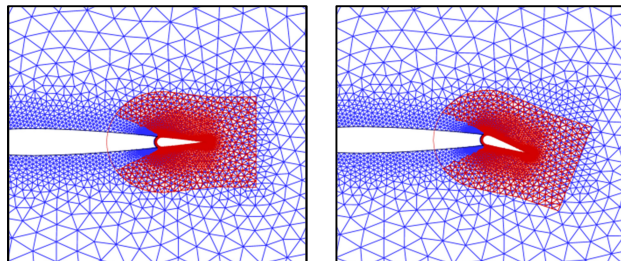


Figure 3: Assembled Chimera mesh for a NACA0012 airfoil with movable flap. Left: mesh without deflection. Right: Mesh component for the flap rotated 20°.

## 3. ALTERNATIVE METHODS

### 3.1. Mesh deformation combined with the Chimera technique

If no large control surface deflections are considered (for instance $\delta < 30°$), combining mesh deformation and the Chimera technique allows to overcome some of the drawbacks that each of the "pure" methods has. In particular, it is possible to model the spanwise gaps without a gap in flow direction.

The combination of these two approaches makes necessary to consider a new mesh set-up. Now, a mesh for a wing and a single control surface is made of at least 4 mesh blocks, see figure 4. The main mesh corresponds to the wing, while the remaining meshes model the control surface and the two spanwise gaps. The mesh for the control surface is deflected through mesh deformation and not through a rigid rotation, so a gap in flow direction is no longer necessary. This is a significant simplification in the mesh generation process which results in a reduction of nodes and the time to generate the mesh. In figure 4 it can
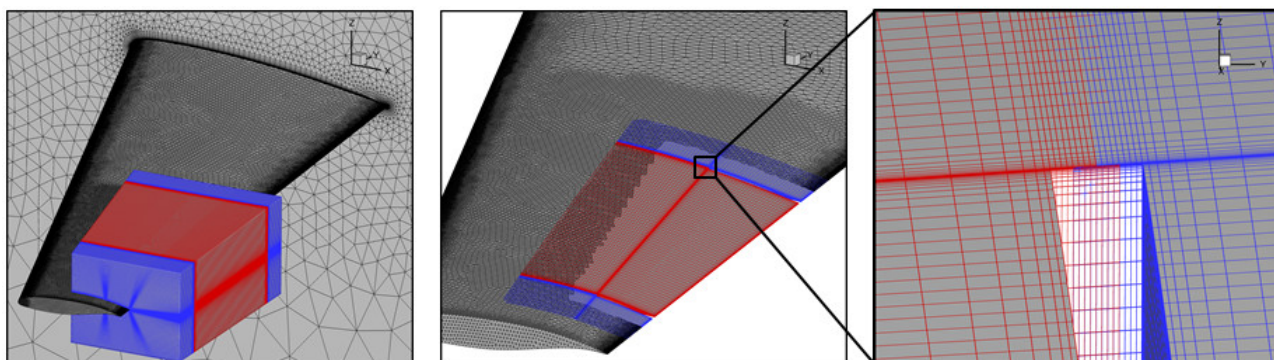


Figure 4: Mesh set-up for the combination of mesh deformation and the Chimera technique. Left: Assembled mesh, consisting of an unstructured mesh for the wing and three structured meshes for the control surface. The two blue structured meshes are fixed; the middle structured mesh is deformed through mesh deformation. Middle: Detail of the mesh closer to the control surface. The wing mesh has been refined in the area of the control surface to achieve a valid Chimera overlap, and the nodes placed inside the hole have been blanked. Right: Detail of the Chimera overlap for two of the structured meshes.

be seen that the meshes for the control surface and the gaps are structured. This offers an easier modelling of the gap area because chopping of the elements close to the wall is avoided. In addition, it is easier to achieve the sufficient mesh overlap necessary for the Chimera technique, because the size of the elements can be easily controlled. Using structured meshes also provides a better resolution of the wake behind the control surface. Nevertheless, combining unstructured and structured meshes requires using two different mesh generation softwares.

A comparison between "pure" mesh deformation, "pure" Chimera technique and a combination of mesh deformation and Chimera technique can be found in [8]. As shown there, the latter method is the best one in terms of computational time and solution accuracy. However, the mesh generation process is still cumbersome due to the overlapping requirements of the Chimera technique.

### 3.2. Mesh deformation combined with sliding interfaces

Despite the good performance of the Chimera technique combined with mesh deformation, the mesh generation process is still complicated. Usually, the final assembled meshes have a large number of nodes, especially in complex configurations with narrow gaps, so they are not suitable for e.g. filling an aerodynamic database or performing manoeuvre simulations. Therefore, it is desired to develop an alternative method which does not require an overlap.

There has been much attention devoted to efficient methods for simulation of relative grid motion which do not require overlapping of the primary mesh, in particular for turbomachinery applications. Nowadays, many methods based on sliding mesh boundaries can be found in the literature. A popular approach consists in using ghost nodes, usually also called halo nodes. Nodes from each mesh component are extrapolated onto the opposite side of the interface. In [9], this is made through an extrusion of the elements along the interface, i.e., an overlapping area of one prismatic layer of ghost cells is generated during the flow computation. The method presented in [10] does not create any overlapping elements, and the ghost nodes are used to compute the flow variables at the interface by means of linear interpolation.

In this work, an alternative sliding interfaces approach based on the computation of the flux across the interface between two mesh components is presented. The method has been implemented in TAU as a new boundary condition, and works similarly to the DLR´s next generation CFD code FLUCS (Flexible Unstructured CFD Software), see [11] for more details.

Figure 5 shows a general non-conforming interface between two mesh blocks named I and II. Although not shown here, relative sliding movement between the grid blocks is also possible. At each iteration of the flow solver, the fluxes across the cell faces at the interface are Independently computed on both sides by means of a Riemann solver. Therefore, a "left" flow state and a "right" flow state have to be defined. Let $W_L$ be the flow data vector of the mesh block I, i.e., $W_L$ defines the so-called "left" state. TAU is a vertex-centred code, so the values of $W_L$ are stored directly at the nodes of the mesh block I. In the case of a non-conforming interface, the corresponding

"right" state, $W_R$, is computed in the following way:

1. For a given inner node located on the boundary face of block I, define a matching ghost node, as shown in figure 6.

2. In block II, locate the inner nodes that are placed above (A) and below (B) the ghost node, as shown in figure 7.

3. Compute the value of $W_R$ at the virtual node by means of linear interpolation using the flow data from the inner nodes A and B.

If the problem is defined for an inner node of block II, the computation of $W_L$ at the corresponding virtual node is made in an equivalent way using the inner nodes from block I for interpolation.

After setting $W_L$ and $W_R$, a Riemann solver is used to compute the flux across the interface between the two mesh blocks. In TAU, this is done with the modified Advection Upstream Splitting Method (AUSM) proposed by [12]. In case of Low-Mach preconditioning, a method based on the MAPS++ upwind scheme [13] can be used.
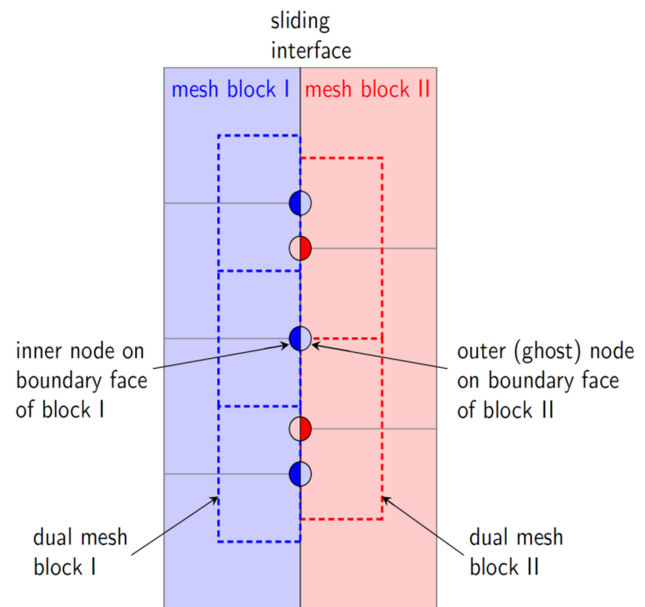


Figure 5: Definition of a non-conforming general interface between two mesh blocks I and II.
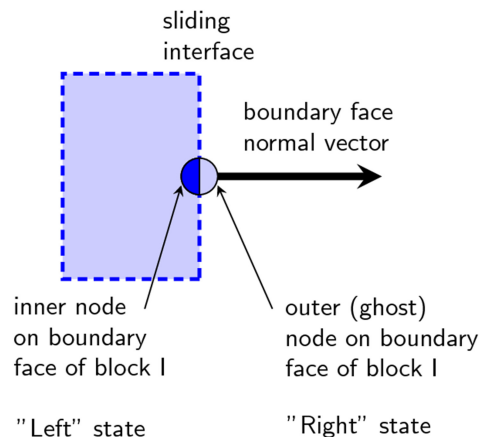


Figure 6: Definition of a ghost node corresponding to a real inner node for the mesh block I.
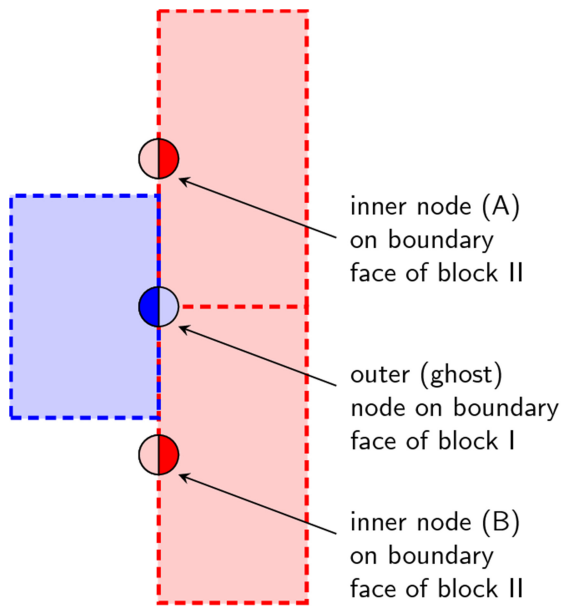
Figure 7: Inner nodes of block II located above and below the ghost node of block I.

## 4. TEST CASES

In what follows, the two alternative methods for modelling of control surfaces are applied to different test cases. First of all, a simulation of the Prandtl-Meyer expansion is used to verify the sliding interfaces boundary condition. The second study considers a LANN wing with four different spanwise gap sizes. The goal is to investigate how the size of the gap influences the aerodynamics of the wing, and also to find the optimal size that yields to realistic results. The conclusions of this study are used to model the different control surfaces of the so-called DLR MULDICON configuration.

### 4.1. Prandtl-Meyer expansion fan

The supersonic expansion of an inviscid flow over a convex corner is a well-known simple two-dimensional problem that has been used to test and verify the implementation of the sliding interfaces boundary condition. The expansion fan ($Ma_\infty = 1.5$) has been simulated using a standard Cartesian mesh as reference, and the corresponding result has been compared to the ones obtained using two meshes for sliding interfaces. These meshes are made of two mesh blocks and the interface between them is conforming and non-conforming, respectively. The non-conforming mesh is shown in figure 8.

Figure 9 presents the results of the flow simulations for both the reference mesh and the meshes for sliding interfaces. As it can be seen, there is a good agreement between the reference solution and the solutions obtained with the sliding interfaces boundary condition, both for the conforming and the non-conforming interface. This verifies the boundary condition for steady applications. Additional investigations proved that the method is also suitable for performing dynamic simulations like for example movable control surfaces, where the position of the mesh nodes at the interface changes at each time step.
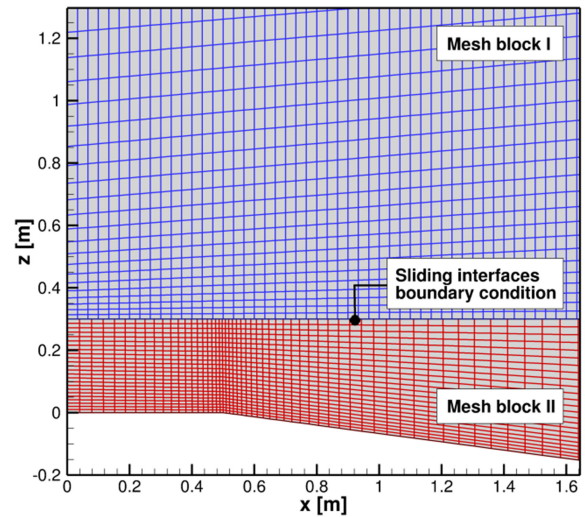


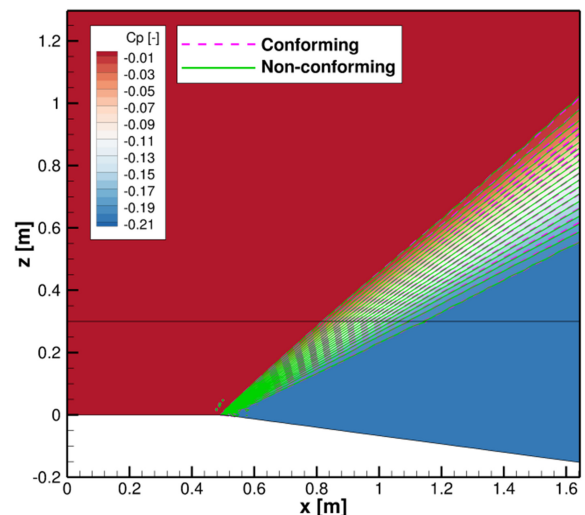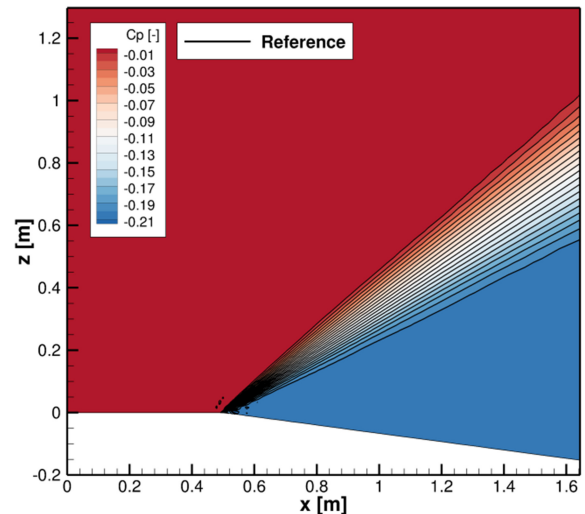Figure 8: Mesh for a non-conforming interface.





Figure 9: Computation of the Prandtl-Meyer expansion fan Top: Reference solution. Bottom: Sliding interfaces solution for a conforming and a non-conforming interface.

5

## 4.2.   LANN wing

The simulation of movable control surfaces with narrow spanwise gaps is a challenging task. On the one hand, modelling a big gap simplifies generating a mesh with good quality but will lead to large aerodynamic losses. On the other hand, smaller gaps are closer to the ones existing in real aircraft and will deliver more reasonable results, but the quality of the mesh in the gap area might be an issue during the flow computation. Therefore, a compromise between accuracy of the results and stability of the simulation has to be found. The following study aims to find out a reasonable gap size that does not yield to large aerodynamic losses by studying how different gap sizes influence the lift coefficient distribution of a wing.

Table 1 presents four test cases based on the LANN wing [14] geometry with a generic aileron shown in figure 10. The size of the gaps is given in terms of the reference length $C_{ref}$ at the wing root, which is equal to 1000 mm.
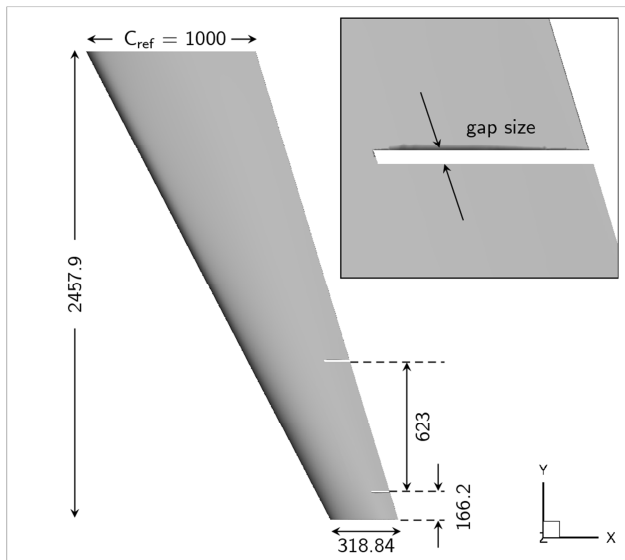


Figure 10: LANN wing with a generic aileron. All sizes are given in mm.

| Test case | 1 | 2 | 3 | 4 |
|---|---|---|---|---|
| Gaps size | - | 1%$C_{ref}$ | 0.1%$C_{ref}$ | 0.01%$C_{ref}$ |
| Gaps size [mm] | - | 10 | 1 | 0.1 |

Table 1: Definition of the different test cases.

The first test case consists in a "clean" geometry without spanwise gaps. For this geometry a standard mesh has been generated with the mesh generation software CENTAUR [15]. The meshes for the test cases 2 and 3 are made of two mesh blocks which have been generated with the modular approach from CENTAUR. For the test case 4, the gaps are too narrow and it has not been possible to generate a valid mesh.

Computations have been performed for $Ma_\infty = 0.3$, $Re_\infty = 30 \cdot 10^6$ and $\delta = 0°$. All simulations have been carried out with the negative version of the Spalart-Allmaras model [16], which is the standard one-equation turbulence model in TAU. The clean geometry is taken as reference,

so in order to find out the effect of the size of the gaps, the following error in terms of $C_L$ is defined:

(1)
$$e_{C_L} = \frac{|C_{L,\text{no gap}} - C_{L,\text{gap}}|}{|C_{L,\text{no gap}}|}$$

Table 2 summarizes the error values for the two gap sizes that have been considered. As it could be expected, the error is smaller for the geometry with the narrowest gap. This trend is confirmed in figure 11 for the lift distribution for $\alpha = 0°$. The error also diminishes when the angle of attack is increased both for a gap size equal to 1%$C_{ref}$ and 0.1%$C_{ref}$, that is, the effect of the gaps is less important for greater angles of attack. In the case of the narrowest gap, the computations for $\alpha = 12°$ and $\alpha = 14°$ are not fully converged, this is probably due to unsteady flow phenomena.

| $\alpha$ [°] | $e_{C_L, gap=1\%C_{ref}}$ [%] | $e_{C_L, gap=0.1\%C_{ref}}$ [%] |
|---|---|---|
| 0 | 3.49 | 0.31 |
| 2 | 1.98 | 0.16 |
| 4 | 1.40 | 0.10 |
| 6 | 1.09 | 0.06 |
| 8 | 0.88 | 0.03 |
| 10 | 0.72 | 0.01 |
| 12 | 0.57 | - |
| 14 | 0.08 | - |

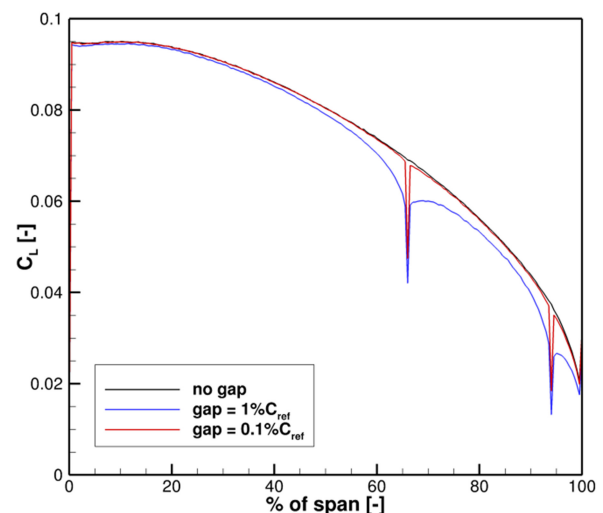Table 2: Error in $C_L$ for different values of $\alpha$.



Figure 11: Lift distribution for $\alpha = 0°$.

In theory, smaller values of $e_{C_L}$ could be expected for a gap size equal to 0.01%$C_{ref}$, but, as mentioned before, unfortunately no valid mesh could be generated. Since for the gap size equal to 0.1%$C_{ref}$ the values of $e_{C_L}$ are beyond 1%, this gap size is a reasonable choice for

realistic simulations.

## 4.3. DLR MULDICON configuration

The combination of the Chimera technique and mesh deformation has been applied to model the control surfaces of the so-called MULti DIsciplinary CONfiguration (MULDICON), a generic Unmanned Combat Air Vehicle (UCAV) developed for research purposes, see figures 13 and 14. This flying wing configuration has been designed as a further development of the DLR-F19 configuration [17] within the DLR project Mephisto.
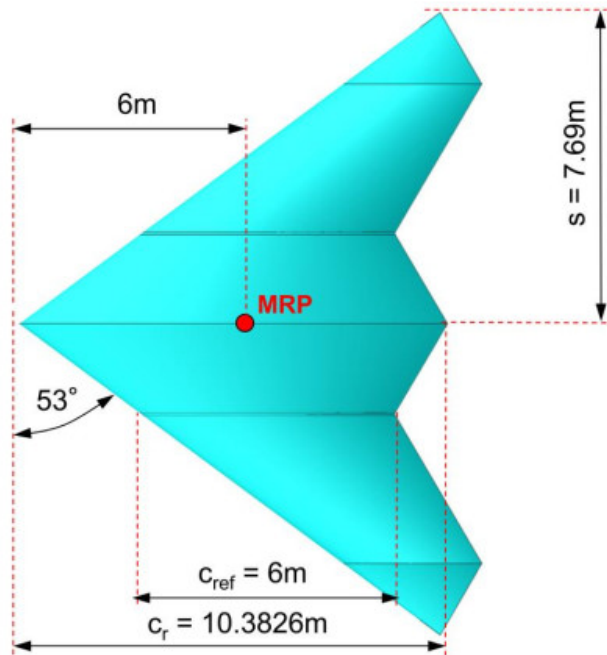


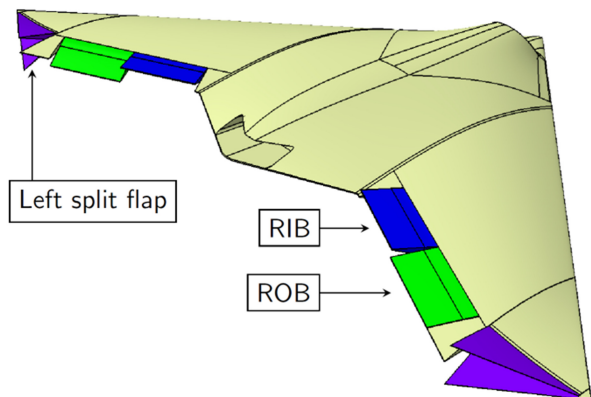Figure 13: Planform and reference data for the MULDICON configuration.



Figure 14: Control surfaces of the MULDICON configuration.

Figure 14 shows the MULDICON control surfaces that have been considered in this work. They are the Right Inboard (RIB) elevon, the Right Outboard (ROB) elevon and the left split flap on the wingtip. In consistency with the results provided by the LANN wing test cases, the size of the spanwise gaps between the control surfaces and the wing is equal to $0.1\%c_{ref}$. All computations have been performed at $Ma_\infty = 0.4$, $Re_\infty = 55.8 \cdot 10^6$ and the negative Spalart-Allmaras turbulence model has been

used. For simplicity reasons, the engine has not been taken into account, i.e., the geometry is "clean" and the engine inlet and outlet from figure 14 are not considered.

### 4.3.1. Deflection of the RIB and ROB elevons

Figure 15 shows a Chimera mesh for one half of the MULDICON configuration which is made of five component grids. The wing grid is unstructured and has been generated with CENTAUR. The additional four structured grids model the RIB and ROB control surfaces and have been generated with POINTWISE [18]. As it has been already said, the generation of a valid Chimera mesh is usually difficult for complex configurations. In the case of the MULDICON configuration, several refinements were necessary to achieve a sufficient overlap in the spanwise gaps area. The first generated mesh with an insufficient overlap had $21.1 \cdot 10^6$ nodes while the final grid has $53.2 \cdot 10^6$ nodes, so the number of nodes grew more than two times.
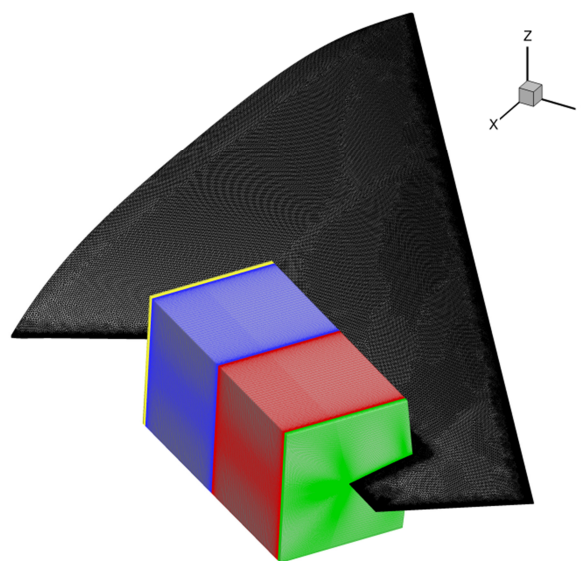


Figure 15: Chimera mesh of the MULDICON half configuration including the RIB and ROB control surfaces.

It is not efficient to use this Chimera mesh to perform dynamic simulations due to its large number of nodes, so an alternative mesh suitable for the sliding interfaces boundary condition was generated. Since no overlapping between the mesh components is required, the new mesh could be easily generated and has a much lower number of nodes, see table 3. This mesh is unstructured and was generated with the modular approach from CENTAUR.

| $\delta$ [°] | Standard | Chimera | Sliding interfaces |
|---|---|---|---|
| 0 | $18.1 \cdot 10^6$ | | |
| | | $53.2 \cdot 10^6$ | $17.6 \cdot 10^6$ |
| 10 | $20.1 \cdot 10^6$ | | |

Table 3: Mesh nodes for one half of the MULDICON configuration.

For completeness and verification of the results, two standard meshes, that is, meshes made after deflecting the control surfaces in the CAD geometry, have been generated using CENTAUR. The number of nodes for each mesh is also given in table 3, and the corresponding

results are taken as a reference.

Figures 16 and 17 compare the $C_p$ distribution computed using the standard meshes, a Chimera mesh and a mesh for sliding interfaces with 0° and 10° deflection of the RIB and ROB elevons, respectively. In all cases, $\alpha = 2°$. Except in the standard case, mesh deformation has been used to deflect the two control surfaces. The results show that there is a good agreement between the Chimera and the sliding interfaces results, so the latter approach can be considered suitable for modelling complex configurations like the MULDICON.

Nevertheless, minor differences can be found for the deflected configuration, in particular close to the spanwise

gaps. This is due to the usage of structured meshes in the Chimera computation, which provide better quality elements in the gaps area. The deviation between the results is increased if the control surfaces are deflected with mesh deformation, since the unstructured mesh is more likely to have bad quality elements close to the gaps.

Another effect of mesh deformation can be seen on the lower surface of the RIB and ROB elevons, see the $C_p$ slices from figure 17. The results of Chimera and sliding interfaces are similar, but they do not perfectly agree with the ones computed with the standard mesh, in particular in the area close to the main wing. This could be expected because the elevons are deflected in the CAD software,
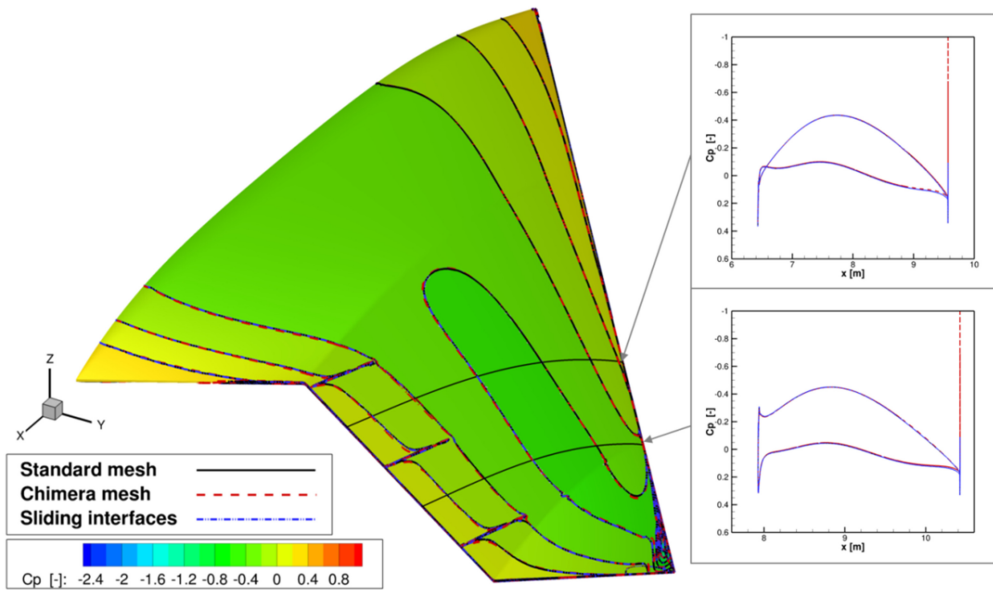


Figure 16: $C_p$ distribution obtained with a standard mesh, a Chimera mesh, and a sliding interfaces mesh for $\delta_{RIB} = \delta_{ROB} = 0°$.
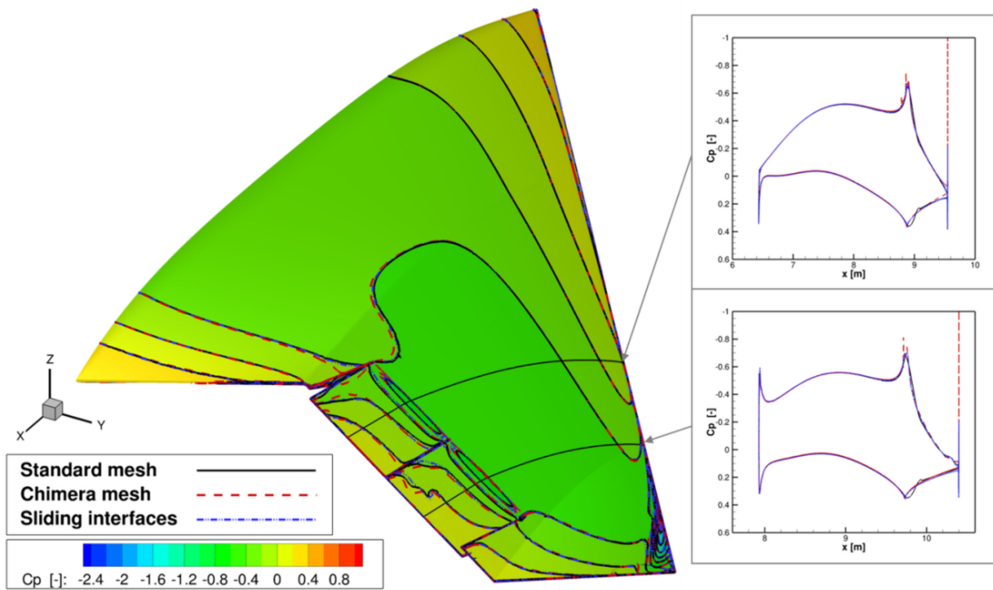


Figure 17: $C_p$ distribution obtained with a standard mesh, a Chimera mesh, and a sliding interfaces mesh for $\delta_{RIB} = \delta_{ROB} = 10°$.

i.e., the geometry is more accurate. However, the agreement between the results is much better on the upper surface, in particular between the standard mesh and the sliding interfaces mesh, which have the same type of elements.

### 4.3.2. Deflection of the split flap

One of the challenges of the MULDICON design process is to keep the radar cross section low. The deployment of the control surfaces should be as small as possible, and the configuration does not have a vertical tail plane [19]. Taking this into account, investigations on the controllability of the configuration have been carried out in recent years, in particular regarding yaw control devices [20]. Among other concepts, a split flap on the wingtip of the MULDICON has been studied. According to the results of the simulations with the RIB and ROB elevons, the sliding interfaces method is the most suitable one for performing numerical simulations with the split flap.

The computational mesh is unstructured and has $62.4 \cdot 10^6$ nodes. As shown in figure 18, it consists in a main mesh block for the wing (drawn in yellow), a mesh block around the tip area (in green) and a mesh block for the split flap which is inside the former one (in pink). This mesh set-up defines an external interface between the main block and the block around the tip area; and an internal one between the block around the tip area and the block for the split flap. The internal interface allows simulating the split flap deflection, while the external interface is useful to avoid remeshing of the main wing in case the geometry of the split flap is redesigned. If there were only the main wing block and the split flap block, a change in, for instance, the hinge line, would require modifying the shape of the interface between the blocks, so a complete new mesh would need to be generated. If there are two interfaces, only the internal one needs to be regenerated and the external interface remains unchanged, so the mesh for the main wing can be kept and additional computational costs can be avoided. Figure 19 presents the results of the split flap simulations using sliding interfaces combined with mesh deformation. The original position of the upper flap is $\delta_{UP} = 45°$, the lower flap one is $\delta_{DOWN} = 32°$. Successful computations have been done for $\alpha = 4°$, $\delta_{UP} \in [35°, 60°]$ and $\delta_{DOWN} \in [17°, 32°]$.

### 5. CONCLUSIONS

In this work, the different methods for modelling movable control surfaces with CFD that are available at DLR have been presented. The first method, which consists in generating a new mesh for each deflection angle of the control surfaces, is not suitable for dynamically moving control surfaces and should primarily be used to verify the alternative methods for the modelling of control surfaces. Then, the usage of pure RBF mesh deformation and the pure Chimera technique are considered. Nevertheless, the former method does not provide realistic results for great deflection angles, because it cannot model the spanwise gaps between the control surface and the wing, hence the shape of the deployed geometry is not realistic. The pure Chimera technique can model the spanwise gaps, but an additional gap in flow direction needs to be considered. Another alternative method combines the Chimera technique and mesh deformation. Although this approach provides good results, the mesh generation is a cumbersome process. In particular, the Chimera technique requires an overlap between the different mesh blocks,
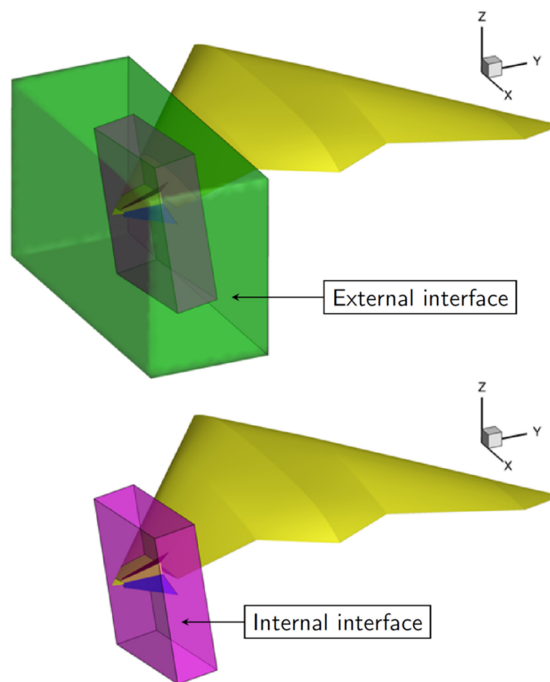


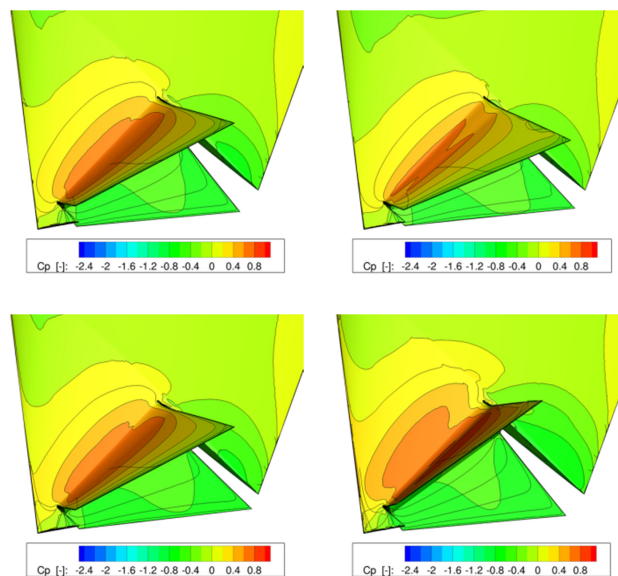Figure 18: Set-up of the mesh components for the MULDICON configuration with split flap.



Figure 19: Deflection of the left split flap of the MULDICON. Top, left: $\delta_{UP} = 45°$, $\delta_{DOWN} = 32°$ (original geometry). Top, right: $\delta_{UP} = 45°$, $\delta_{DOWN} = 17°$. Bottom, left: $\delta_{UP} = 60°$, $\delta_{DOWN} = 32°$. Bottom, right: $\delta_{UP} = 35°$, $\delta_{DOWN} = 22°$.

and this can dramatically increase the number of nodes of the mesh, especially in configurations with narrow spanwise gaps.

In order to overcome the drawbacks of the previous methods, an approach based on a combination of a sliding interfaces boundary condition and mesh deformation is suggested. The flow solution is obtained by solving a Riemann problem at the interface between the mesh blocks, so an overlap is no longer required. This new boundary condition is verified with a Prandtl-Meyer

expansion. Then, the influence of the size of the spanwise gaps on the lift coefficient of a LANN wing is studied, and it is shown that a suitable gap size is equal to $0.1\%C_{ref}$.

Computations involving the MULDICON configuration are also performed. The RIB and ROB elevons are deflected up to 10° using a standard mesh, a Chimera mesh and a mesh for sliding interfaces. The good agreement between the different results shows that the sliding interfaces method is the most suitable one for complex configurations like the MULDICON. The results also point out that using a structured mesh for the control surfaces results in more accurate results, especially regarding the flow close to the gaps. Therefore, further computations could be made using sliding interfaces and structured meshes for the control surfaces. Finally, simulations for the left split flap of the MULDICON are done for $\delta_{UP} \in [35°, 60°]$ and $\delta_{DOWN} \in [17°, 32°]$. The computations are performed with the sliding interfaces method, and the mesh can be used to change the geometry of the split flap without great user effort.

## 6. ACKNOWLEDGMENTS

## REFERENCES

[1] N. Kroll, M. Abu-Zurayk, D. Dimitrov, T. Franz, T. Führer, T. Gerhold, S. Görtz, R. Heinrich, C. Ilic, J. Jepsen, J. Jägersküpper, M. Kruse, A. Krumbein, S. Langer, D. Liu, R. Liepelt, L. Reimer, M. Ritter, A. Schwöppe, J. Scherer, F. Spiering, R. Thormann, V. Togiti, D. Vollmer and J.-H. Wendisch, "DLR Project Digital-X: Towards Virtual Aircraft Design and Flight Testing Based on High-Fidelity Methods", CEAS Aeronautical Journal, Vol. 7, No. 1 (2016), pp- 3-27.

[2] N. Kroll, S. Langer and A. Schwöppe, "The DLR Flow Solver TAU – Status and Recent Algorithmic Developments", 52th AIAA Aerospace Sciences Meeting, National Harbor, Maryland, USA, 2014.

[3] A. Michler, "Aircraft control surface deflection using RBF-based mesh deformation", International Journal for Numerical Methods in Engineering, Vol. 88, No.10 (2011), pp. 986-1007.

[4] D.R. McDaniel, D.R. Sears, T.R. Tucky, B. Tillman and S.A. Morton, "Aerodynamic control surface implementation in kestrel v2.0", 49th AIAA Aerospace Sciences Meeting including the New Horizons Forum and Aerospace Exposition, Orlando, Florida, USA, 2011.

[5] A. Madrane, A. Raichle, A. Stürmer, "A Parallel Implementation of a Dynamic Overset Structured Grid Approach", Proceedings of the European Conference on Computational Fluid Dynamics, Jyväskylä, Finland, 2004.

[6] N. Liggett and M. J. Smith, "The physics of modelling unsteady flaps with gaps", Journal of Fluids and Structures, Vol. 38 (2013), pp- 255-272.

[7] F. Spiering, "Development of a Fully Automatic Chimera Hole Cutting Procedure in the DLR TAU code", New Resulrs in Numerical and Experimental Fluid Mechanics X Notes on Numerical Fluid Mechanics and Multidisciplinary Design, Vol. 132 (2016), pp. 585-595.

[8] L. Reimer and R. Heinrich, "Modeling of Movable Control Surfaces and Atmospheric Effects", Computational Flight Testing Notes on Numerical Fluid Mechanics and Multidisciplinary Design, Vol. 121 (2013), pp. 183-206.

[9] E.L. Blades and D.L. Marcum, "A sliding interface method for unsteady unstructured flow simulations", International Journal for Numerical Methods in Fluids, Vol. 53, No. 3 (2007), pp.507-529.

[10] J. McNaughton, I. Afgan, D.D. Apsley, S. Rolfo, T. Stallard and P.K. Stansby, "A simple sliding-interface procedure and its application to the CFD simulation of a tidal-stream turbine", International Journal for Numerical Methods in Fluids, Vol. 74, No. 4 (2014), pp. 250-269.

[11] T. Leicht, D. Vollmer, J. Jägersküpper, A. Schwöppe and R. Hartmann, "DLR-Project Digital-X – Next Generation CFD Solver Flucs", Deutscher Luft- und Raumfahrtkongress, Braunschweig, Germany, 2016.

[12] N. Kroll and R. Radespiel, "An improved flux vector split discretization scheme for viscous flows", DLR-FB 93-53, 1993.

[13] C.-C. Rossow, "A flux splitting scheme for compressible and incompressible flows", Journal of Computational Physics, Vol. 164 (2000), pp. 104-122.

[14] R.J. Zwann, "Data set 9, LANN wing. Pitching oscillation", Agard-R-702 Addendum No. 1, AGARD; Amsterdam, The Netherlands, 1985.

[15] CENTAUR Mesh Generation Software, "http://www.centaursoft.com".

[16] S.R. Allmaras, F.T. Johnson and P.R. Spalart, "Modifications and Clarifications for the Implementation of the Spalart-Alllmaras Turbulence Model", 7th International Conference on Computational Fluid Dynamics (ICCFD7), Big Island, Hawaii, USA, 2012.

[17] K.C. Huber, D.D. Vicroy, A. Schütte and A.R. Hübner, "UCAV model design and static experimental investigations to estimate control device effectiveness and Stability and Control capabilities", AIAA Applied Aerodynamics Conference, Atlanta, Georgia, USA, 2014.

[18] POINTWISE Mesh Generation Software, "http://www.pointwise.com".

[19] C.M. Liersch, K.C. Huber, A. Schütte, D. Zimper and M. Siggel, "Multidisciplinary design and aerodynamic assessment of an agile and highly swept aircraft configuration", CEAS Aeronautical Journal, Vol. 7, No. 4 (2016), pp. 677-694.

[20] P. Löchert, K.C. Huber, C.M. Liersch and A. Schütte, Control device studies for yaw control without vertical tail plane on a 53° swept flying wing configuration, AIAA Applied Aerodynamics Conference, AIAA AVIATION Forum, Atlanta, Georgia, USA, 2018.